PHYSICAL REVIEW B VOLUME 56, NUMBER 5 1 AUGUST 1997-I

Geometrical locking of the irreversible magnetic moment to the normal of a thin-plate superconductor

A. A. Zhukov
Physics Department, Moscow State University, Moscow 117234, Russia and Centre for High Temperature Superconductivity, Blackett Laboratory, Imperial College, London SW7 2BZ, United Kingdom

G. K. Perkins, Yu. V. Bugoslavsky,* and A. D. Caplin
Centre for High Temperature Superconductivity, Blackett Laboratory, Imperial College, London SW7 2BZ, United Kingdom
(Received 21 January 1997)

We solve the Bean critical-state model for the screening current distribution in an infinite superconducting slab in a tilted magnetic field **H**, and calculate from it the magnitude and direction of the induced magnetic moment **m**. As the tilt angle increases, **m** remains directed close to the plate normal **n** until **H** is almost perpendicular to **n**, then **m** rotates very rapidly. We consider several generalizations of the model: finite length, a more realistic current-voltage characteristic, and critical-current anisotropy, but find that they have only a minor quantitative effect on the results derived for the simplest case. Also, we prove that the closure currents always contribute half the moment. Vector magnetic moment measurements of $YBa_2Cu_3O_y$ single crystals and an epitaxial film, and also on samples of conventional superconductors, confirm the model calculations. These geometrical effects are important for the analysis of the angular behavior of the critical currents and their anisotropy in HTS materials; also, they assist the observation of vortex locking to twin boundaries in HTS crystals, but tend to obscure vortex locking to CuO planes. [S0163-1829(97)04929-1]

I. INTRODUCTION

A characteristic feature of high-temperature-superconductor (HTS) single crystals is their thin platelike shape. Many studies have reported observations of a large anisotropy in the irreversible magnetization (generated by screening currents) of such crystals, and often this has been interpreted in terms of the intrinsic anisotropy of the materials (e.g., Refs. 1–3).

However, as has been pointed out previously,[4,5] geometric effects contribute strongly to this anisotropic angular behavior. In a platelike *isotropic* superconductor, the direction of the irreversible magnetization is almost independent of the angle of the applied field, and remains closely parallel to the smallest sample dimension until the field is oriented almost parallel to the plane of the plate (we are interested here in applied fields much larger than the self-fields generated by the screening currents, so that classical demagnetizing factors are unimportant). Consequently, because of the usual sample shape of HTS crystals, it is difficult to extract and quantify their intrinsic anisotropy of screening currents and vortex behavior. Note that the *reversible* magnetization arising from equilibrium Meissner currents is affected by demagnetizing factors, but not by these additional complications, so its anisotropy is much more straightforward to interpret. The geometrical effects considered here are important at all fields where irreversibility exists, whereas the reversible magnetization and its demagnetizing fields are significant only at low fields, up to $\sim H_{c1}$.

These qualitative conclusions about geometrical effects on the irreversible magnetization have not previously been substantiated by quantitative analysis. Here we present the solution of the Bean critical state model for an infinite thin slab of a superconductor in a tilted magnetic field, and then consider extensions toward a more realistic description of the situation (Sec. II). In Sec. III we compare the results of the calculations with detailed experimental measurements of the vector magnetic moment of both HTS crystals and platelets of conventional superconductor, obtained using a vibrating sample magnetometer (VSM) equipped with two orthogonal coil sets. We then examine the impact of these geometrical effects in HTS crystals (Sec. IV), particularly on measurement and analysis of the anisotropy of the critical current and of different kinds of pinning mechanism, and also on the putative identification of ''vortex-locking'' phenomena.

II. THEORY

The key factors that make the analysis of the screening current distribution in a realistic superconducting sample difficult are the three-dimensionality of the problem, the loss of symmetry when the applied field is directed away from a principal axis, and the form of the E-j characteristic. We therefore start with the simplest case, the Bean model for an infinite slab, and then examine extensions to it.

A. The Bean model for an infinite slab in tilted magnetic field

1. The model

The essence of the Bean model is that the screening current density j has the same magnitude j_c everywhere, and a sign given by that of the local electric field E; this corresponds to a threshold current-voltage characteristic $\mathbf{j} = j_c \mathbf{E}/E$. As in the original model[6] we take j_c to be independent of both the magnitude and direction of the local induction **B** within the sample. Also, we restrict the analysis to large applied magnetic fields **H**, so that the self-field

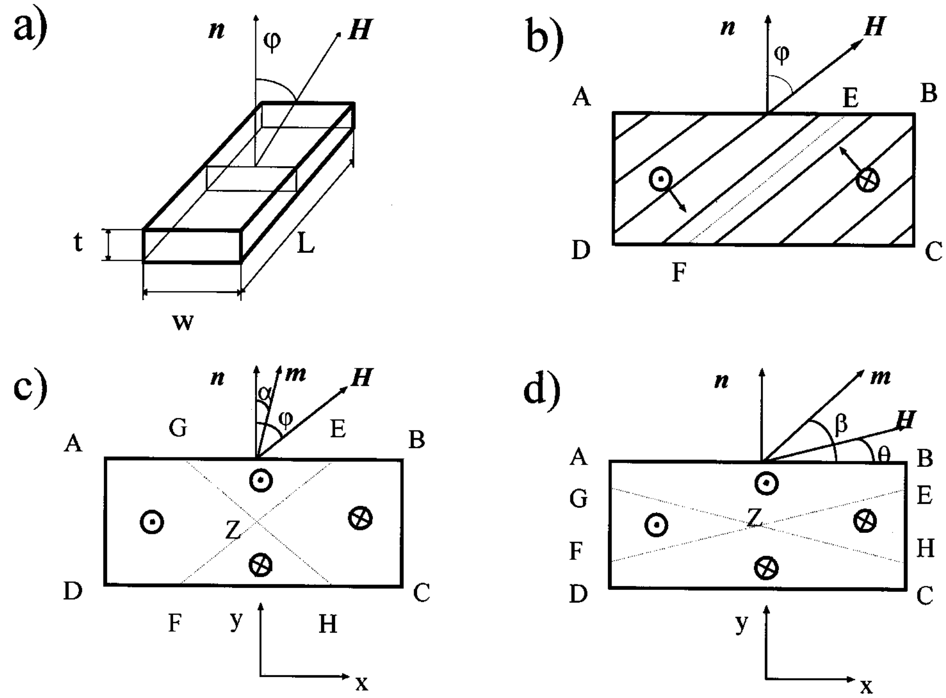

FIG. 1. (a) Geometry for calculation of the Bean model in a tilted magnetic field; (b) directions of screening currents (⊙ and ⊗) and of the Lorentz force (arrows) on the vortices (thick lines) in a cross section of the sample; (c) the screening current distribution for $\varphi<\varphi_c$; (d) the screening current distribution for $\varphi>\varphi_c$.

created by the shielding currents can be neglected; then within the slab, we may put $\mathbf{B}=\mu_0\mathbf{H}$, and the vortices are straight and parallel to **H**.

Even within these restrictions, it is difficult to obtain a solution in closed form for a rectangular plate of finite length because the closure currents at the ends destroy the translational invariance. We therefore consider an infinite thin slab, as the limiting case of a long plate [Fig. 1(a)] of length L much larger than its width w or thickness t, so effectively reducing the three-dimensional problem to two-dimensions. The aspect ratio κ $(=w/t)$ of the cross section is the key parameter for further analysis.

Let the direction of the magnetic field be rotated in the transverse plane from the plate normal **n** by an angle φ [Fig. 1(a)]. For an infinite slab, translational invariance requires that every cross section be equivalent, and that **B** remains in the transverse plane. Therefore, with increasing **H**, vortices enter from the corners A and C [Fig. 1(b)], move toward the center of the sample, and meet at the plane EF.[4] By symmetry, the screening currents flow in the z direction along the length of the slab. The Lorentz force on the vortices, and so also their drift velocity, is in the xy plane, but has opposite sign on either side of the plane EF. Consequently, the current distribution is antisymmetric with respect to the plane EF, as was first derived by a similar analysis in Ref. 4. This conclusion, based on symmetry, yields the same result as the direct solution of Maxwell's equations (Appendix B).

The behavior of the magnetic moment is different for φ being less than or greater than φ_c $(=\arctan\kappa)$, the direction of the diagonal DB of the transverse cross section of the slab, so we consider these two cases separately.

2. H directed away from the plane of the plate, $\varphi\leqslant\varphi_c$

We use a Cartesian coordinate system in the rotation plane with y parallel to **n** [Fig. 1(c)]. The magnetic moment **m** of the current distribution is given by $\mathbf{m}=(1/2)\int\mathbf{r}\times\mathbf{j}dV$. For **H** along a symmetry direction of a long plate, the closure currents at the ends are known to give a contribution to **m** equal to that of the currents parallel to the length;[7] in Appendix A we show that this remains true for **H** in any direction. Therefore $m_y=L\int xjdS$, and $m_x=L\int yjdS$, where the integrals are evaluated over the cross section.

By symmetry the region $GEZFH$ [Fig. 1(c)] gives zero contribution to m_y, where the plane represented by the line GH corresponds to a field direction of $-\varphi$. Hence m_y is twice the contribution from the trapezoidal region $AGZFD$:

$$m_y=4L\int_{AGZFD}xj_c dx\,dy=\frac{Lt^3}{12}\,j_c(3\kappa^2-\tan^2\varphi). \tag{1}$$

For m_x the moment comes from the region $GEZFH$:

$$m_x=4L\int_{GEZFH}yj_c dx\,dy=\frac{Lt^3}{6}\,j_c\tan\varphi. \tag{2}$$

The angle α between the moment **m** and the plate normal **n** is given by

$$\tan\alpha=\frac{2\tan\varphi}{3\kappa^2-\tan^2\varphi}. \tag{3}$$

For $\varphi=0$ we have the usual result $m_y=Lj_ctw^2/4$, and, of course, $\alpha=0$. When **H** has rotated to the angle φ_c, the moment has deviated by an angle $\alpha_c=\operatorname{arc}\cot\kappa$, so that $\alpha_c=(\pi/2-\varphi_c)$. For angles small enough that $\tan\varphi\ll\kappa$, the deviation angle $\alpha\approx 2\tan\varphi/3\kappa^2$, and $|\mathbf{m}(\varphi)|\approx m(0)(1-\tan^2\varphi/3\kappa^2)$. Thus, for a plate representing typical HTS crystals, with κ of ~ 10 or more, the irreversible magnetic moment is almost locked to the plate normal for this entire range of applied field directions. At the end of the range, we have that $m_y(\varphi_c)=2m_y(0)/3$ and $m_x(\varphi_c)=m_y(\varphi_c)/\kappa$, so that the modulus of **m** changes rather slowly too.

3. H close to the plane of the plate, $\varphi \geqslant \varphi_c$

In the angular range $\varphi_c \leqslant \varphi \leqslant \pi/2$ [Fig. 1(d)] it is more appropriate to measure the deviation of **H** and **m** from the plane, by the angles $\theta=(\pi/2-\varphi)$ and $\beta=(\pi/2-\alpha)$, respectively. This case maps to the previous solution with the interchanges $x \Leftrightarrow y$, $\varphi \Leftrightarrow \theta$, $t \Leftrightarrow w$, $\kappa \Leftrightarrow 1/\kappa$. Then one can obtain

$$m_x=4L\int_{AGZEB} y j_c dx\, dy=\frac{Lw^3}{12}\, j_c\left(\frac{3}{\kappa^2}-\tan^2\theta\right), \tag{4}$$

$$m_y=4L\int_{EZH} x j_c dx\, dy=\frac{Lw^3}{6}\, j_c \tan\theta, \tag{5}$$

$$\tan\beta=\frac{2\kappa^2\tan\theta}{3-\kappa^2\tan^2\theta}. \tag{6}$$

With **H** (and so **m** also) in the plane of the plate, $|\mathbf{m}| = L j_c w t^2/4$, a factor κ smaller than when the field is normal to it. However, note that small misorientations of **H** induce large angular deviations of **m**: $\beta \approx 2\kappa^2\theta/3$. A useful parameter that describes the rapidity with which **m** rotates as **H** is swung out of the plate plane is

$$\tau=\left(\frac{d\beta}{d\theta}\right)_{\theta=0}=\frac{2\kappa^2}{3}. \tag{7}$$

At the critical angle $\theta_c(=\pi/2-\varphi_c)$ the moment direction is given by $\tan\beta_c=\kappa$, which is identical to the result obtained in Sec. II A 2.

From Eqs. (4) and (5) to lowest order in θ, the modulus of the moment is

$$m(\theta)\approx m(0)\left(1+\frac{2}{9}\,\kappa^4\theta^2\right) \tag{8}$$

and so $|\mathbf{m}|$ increases rapidly with angle.

B. Beyond the Bean model

The steplike current-voltage characteristic that is used in the Bean model is inappropriate for HTS materials in which flux creep is always present, corresponding to j being a smooth function of E. Power laws of the form $E/E_0 =(j/j_0)^n$ provide a much better representation, with n typically in the range 5–30 for HTS crystals, and above 20 for conventional superconductors. The Bean model corresponds to the limit $n\rightarrow\infty$.

In a magnetization experiment, the changing applied magnetic field (which for simplicity we take to be swept at a steady rate $\dot{H}=dH/dt$) induces an electric field. As noted earlier, we are considering the case in which H is much larger than the penetration field, so that the induction generated by the screening currents may be neglected. Furthermore, because **B** is then uniform through the sample, the B dependence of the E-j characteristics may be ignored.

For the infinite slab, a power-law E-j characteristic may be incorporated directly into our previous analysis. As shown in Appendix B, the E field is parallel to z, and has opposite sign on either side of the plane EF of Fig. 1:

$$E_z=\mu_0\dot{H}(x\cos\varphi-y\sin\varphi). \tag{9}$$

Lengthy but straightforward calculations yield, for $\varphi>\varphi_c$ [Fig. 1(d)],

$$m_y=2Lj_0\left(\frac{w}{2}\right)^3\left(\frac{\mu_0\dot{H}w\sin\theta}{2E_0}\right)^{1/n}\tan\theta\,\frac{n^2}{(2n+1)(n+1)} \times\Big\{(a+1)^{2+1/n}+(a-1)^{2+1/n}-\frac{n}{3n+1} \times[(a+1)^{3+1/n}-(a-1)^{3+1/n}]\Big\} \tag{10}$$

and

$$m_x=2Lj_0\left(\frac{w}{2}\right)^3\left(\frac{\mu_0\dot{H}w\sin\theta}{2E_0}\right)^{1/n}\frac{\tan\theta}{\kappa}\,\frac{n^2}{(2n+1)(n+1)} \times\Big\{(a+1)^{2+1/n}-(a-1)^{2+1/n}-\frac{n}{3n+1}\,[(1+a^{-1}) \times(a+1)^{2+1/n}-(1-a^{-1})(a-1)^{2+1/n}]\Big\}. \tag{11}$$

The angle β of **m** from the plane of the plate is now

$$\tan\beta=\frac{2(2n+1)(n+1)a}{6n(n+1)a^2-(2n+1)(n+1)}, \tag{12}$$

where $a=(\kappa\tan\theta)^{-1}$.

These complicated expressions have two interesting limits: For $n\rightarrow\infty$, i.e., the Bean model, they are identical to those obtained in Sec. II A 3. In the Ohmic limit ($n=1$), they simplify greatly to

$$m_y=\frac{Lw^3}{6}\, j_z(0,t/2)\tan\theta, \tag{13}$$

$$m_x=\frac{Lw^3}{6\kappa^2}\, j_z(0,t/2), \tag{14}$$

$$\tan\beta=\kappa^2\tan\theta. \tag{15}$$

These results resemble closely Eqs. (4)–(6), but with the replacement of the Bean model j_c by the current density $j_z(0,t/2)$ flowing at the center of the broad face of the plate. In this orientation of the applied field, $j_z(0,t/2)$ is a good measure of the screening currents that dominate **m**.

The results for angles $\varphi<\varphi_c$ may be obtained directly using the mapping described in Sec. II A 3. Naturally, for $n\rightarrow\infty$ they again reduce to the Bean model. In the Ohmic limit, they yield expressions resembling Eqs. (1)–(3), but involving the current density $j_z(w/2,0)$ flowing at the center of the sides of the plate.

Given that there is very little difference between the results for the Bean and Ohmic limits, we conclude that the behavior of the magnetic moment is insensitive, within numerical factors close to unity, to the precise form of the E-j characteristic, and that the expressions obtained in Sec. II A will generally be adequate.

The critical current is usually strongly dependent on the magnitude and direction of **B**. However, because we are considering the situation in which the effects of self-fields are small, so that **B** is constant within the sample, the dependence of j_z on **B** may be incorporated directly into all the expressions derived so far by replacing it with the value of j_z appropriate to the magnitude and direction of $\mu_0\mathbf{H}$. The direction of **m** [Eqs. (3), (6), (7), and (15)] is unaffected by any dependence of j_z on B.

C. Finite length and closure currents

In the general case of a slab of finite length with the applied field at an arbitrary angle, and an arbitrary current-voltage characteristic, analytic solutions for the screening current distribution are unknown. However, in Appendix B we obtain approximate solutions for the E field in a finite slab, and in the Ohmic case, they can be translated immediately into the current distribution.

From the **E** fields described by Eqs. (B8)–(B10), and using $\mathbf{j}=\sigma E$, we find for the component of $\mathbf{H}\|x$:

$$m_x=\sigma\mu_0\dot{H}_x\,\frac{Lw^3t}{12\kappa^2}\left(1-\frac{t}{4L}\right)=\frac{Lw^3}{6\kappa^2}\,j_z(0,t/2)\left[1+\frac{3t}{4L}+O\left(\frac{t}{L}\right)^2\right] \tag{16}$$

and for the component of $\mathbf{H}\|y$

$$m_y=\sigma\mu_0\dot{H}_y\,\frac{w^3Lt}{12}\left(1-\frac{w}{4L}\right)=\frac{Lt^3}{6}\,j_z(w/2,0)\,\kappa^2\left[1+\frac{3w}{4L}+O\left(\frac{w}{L}\right)^2\right]. \tag{17}$$

In the limit of a long slab, these results (expressed in terms of the current densities at the centres of the slab faces) reduce to those found in the previous section for an Ohmic conductor.

For **H** directed at an angle θ from the x axis, the direction of **m** is given by

$$\tan\beta=\kappa^2\tan\theta\,\frac{1-w/4L}{1-t/4L}. \tag{18}$$

The influence of finite slab length on β can be seen directly by comparison with Eq. (15).

We have shown therefore that, in the Ohmic case, the corrections for finite length are, as might be expected, of order w/L or t/L. In the more realistic situation of a steep power-law E-j characteristic, the magnitude of the correction terms is less obvious. However, we have seen in Sec. II B that for an infinite slab, **m** changes very little between an Ohmic and a Bean E-j characteristic; we propose that the same is true of the corrections to **m** for finite length.

HTS crystals are usually almost square plates, with $L\sim w$, so that the correction to the parameter that is most easily measured, the rotation rate τ when **H** is close to plate plane [Eqs. (7), (15), and (18)], should be no more than about 25%.

III. EXPERIMENTAL INVESTIGATIONS

A. Vector magnetometry

In order to study the key predictions of Sec. II, it is essential to monitor both the magnitude and direction of **m**. We used a vibrating sample magnetometer (Oxford Instruments 5^H) equipped with two independent coil sets that measure simultaneously the magnetic moments parallel (standard component m_{std}) and perpendicular (ortho component m_{ort}) to **H**. The sample can be rotated *in situ* about the third axis, with an angular resolution of 0.01° and reproducibility better than 0.03°. As we have pointed out previously,[8] the sample has to be centered very precisely for the two coil sets to maintain *magnetic* orthogonality.

The data reported here were all obtained as the field was swept steadily around a hysteresis loop, with the sample at fixed orientation; typical sweep rates were ~ 10 mT s^{-1}, and the maximum field was 5 T. In the present context, it is only the irreversible components of **m**, which reflect the behavior of the shielding currents, that are of interest.

B. Samples

We examined $YBa_2Cu_3O_y$ single crystals of several different kinds of dominant pinning. These included twinned and detwinned crystals, and also one containing columnar defects (Table I); their preparation and detwinning have been described elsewhere.[9,10] Different pinning systems affect the anisotropy of j_c in different ways, and so allow us to check the influence of the latter factor on the deviation angle α. For a sample of extreme aspect ratio, we used a $YBa_2Cu_3O_y$ epitaxial film.[11]

For a direct check of the analysis, isotropic superconductors are preferable; we have used polycrystalline samples of conventional superconductors. The Chevrel phase $PbMoS_6$ (No. SV) sample was cut by diamond saw from an ingot; after the first series of measurements, it was cut to decrease the sample width and measured again. The V_3Si sample (No. VS) was cut, measured, thinned on abrasive paper, and measured again.

C. Experimental results and discussion

1. HTS crystals

Figure 2 shows the behavior that is typical of the platelike $YBa_2Cu_3O_y$ single crystals. Over a large angular range, up to $\sim 87°$ from the plate-normal in the No. OZ sample, the direction of the irreversible magnetic moment **m** is locked to the plate normal **n**, so that $\alpha\approx 0°$ (because of the inevitable slight precession of the sample when it is rotated over large angles,[8] there is then an uncertainty in α of about $\pm 1°$). In a narrow angular interval, when the direction of **H** passes through the plane of the plate, **m** flips rapidly through almost 180°, in accord with theory. The data of Fig. 2 are representative of a wide range of fields (provided that **H** is significantly higher than the penetration field $\mathbf{H}_p$) and temperatures, over which the magnitude and anisotropy of j_c change

TABLE I. The measured samples and their characteristics.

Name	Material	Form	Dimensions $L\times w\times t$ (mm)	Aspect ratio, κ	Comments
No. OZ	$YBa_2Cu_3O_y$	Single crystal	$1.95\times1.15\times0.065$	17.7	Twinned, rotation plane $\perp$ to TB
No. MK	$YBa_2Cu_3O_y$	Single crystal	$1.04\times0.97\times0.10$	9.7	Detwinned
No. WZ	$YBa_2Cu_3O_y$	Single crystal	$0.96\times0.90\times0.04$	22.5	Detwinned, high purity
No. AH	$YBa_2Cu_3O_y$	Single crystal	$1.26\times0.57\times0.025$	22.8	Columns $B_\psi=3$ T
No. LF	$YBa_2Cu_3O_y$	Epitaxial film	$2.2\ \times0.9\times0.0003$	3×10^3	
No. SH	$PbMoS_6$	Polycrystal	$2.01\times1.72\times0.40$	4.3	
No. S1	$PbMoS_6$	Polycrystal	$2.01\times0.67\times0.40$	1.68	Cut from No. SH
No. VS	V_3Si	Polycrystal	$6.00\times0.90\times0.35$	2.57	
No. VI	V_3Si	Polycrystal	$6.00\times0.90\times0.27$	3.33	Polished from No. VS

markedly (e.g., Refs. 12–14). Furthermore, for all the $YBa_2Cu_3O_y$ single crystals studied, covering a range of j_c anisotropy because of the different pinning mechanisms present, we observe similar $\alpha(\varphi)$ dependencies that all fit well to the theory of Sec. II evaluated for the measured aspect ratios, and without recourse to fitting parameters. This confirms the dominant role played by geometrical effects in the observed angular behavior of **m**.

The $YBa_2Cu_3O_y$ epitaxial film data (Fig. 3) illustrate the extreme case of the geometrical-locking phenomenon, with **m** flipping its direction within 0.02° rotation of **H**. These data therefore illustrate the angular resolution of the magnetometer.

2. Conventional superconductors

Measurements on conventional superconductors test the geometric theory under rather different and somewhat simpler conditions; in particular, unlike HTS materials, they have no strong anisotropy. This allows us to analyze directly the measured dependence of **m** on φ.

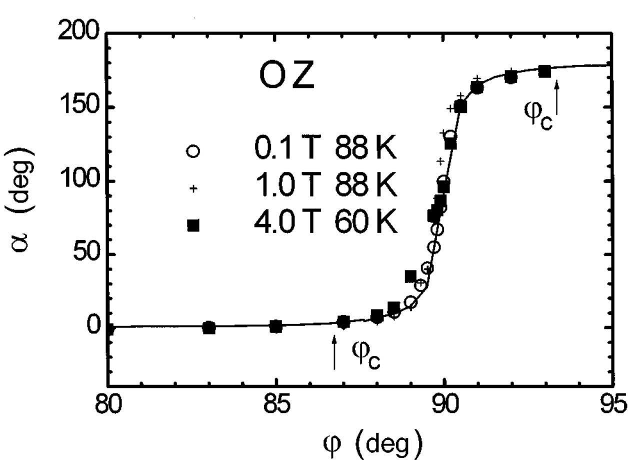

FIG. 2. Angle α of the irreversible magnetic moment from the c axis in a $YBa_2Cu_3O_7$ (sample No. OZ) single crystal for fields applied at angle φ close to the ab plane ($\varphi=90°$) at different temperatures and magnetic fields. The full line shows the fit to Eqs. (3) and (5) calculated for the sample aspect ratio κ of 17.7; the arrows mark the critical angles φ_c.

The measurements of $\alpha(\varphi)$ again show quite good quantitative agreement with theory without use of any fitting parameter (Fig. 4). The variation of the modulus of **m** with φ (Fig. 5) illustrates an important feature: there is the sharp dip in $|\mathbf{m}|$ when the field is nearly parallel to the plate. We emphasize that this minimum is purely geometric in origin, and does not reflect any intrinsic superconducting anisotropy.

The theory of Sec. II A 2 suggests that for φ not close to $\pi/2$, $|\mathbf{m}|$ should be nearly independent of angle; the observed smooth increase as **H** is rotated away from $\varphi=0$ may be connected with metallurgical anisotropy of the sample, or perhaps reflect the limitations of our approximations.

3. The rotation rate τ

A sensitive quantitative test of the geometric model is the rate τ which describes how fast **m** swings round as **H** rotates through the plane of the plate; Eq. (7) predicts that τ should be a simple quadratic function of the aspect ratio κ. The data for both HTS and conventional samples (Fig. 6) fit rather well to this form (the data for the thin film have not been

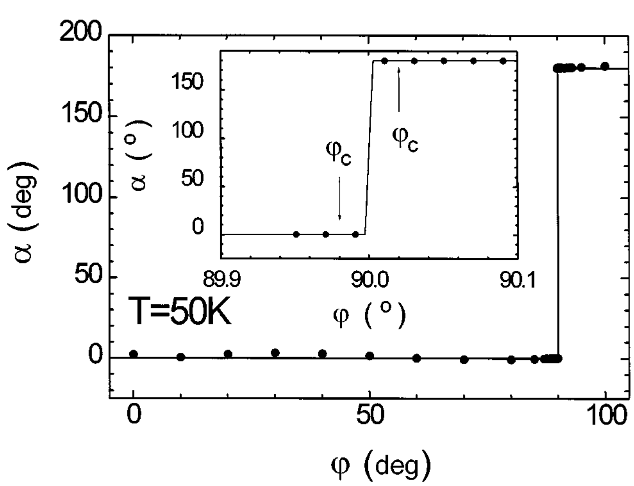

FIG. 3. Measured rotation of the magnetic moment (as in Fig. 2) of a $YBa_2Cu_3O_7$ epitaxial film (No. LF, $T=50$ K, $\mu_0H=0.5$ T) The full line shows the fit to Eqs. (3) and (6) calculated for the sample aspect ratio κ of 3×10^3; the arrows mark the critical angles φ_c.

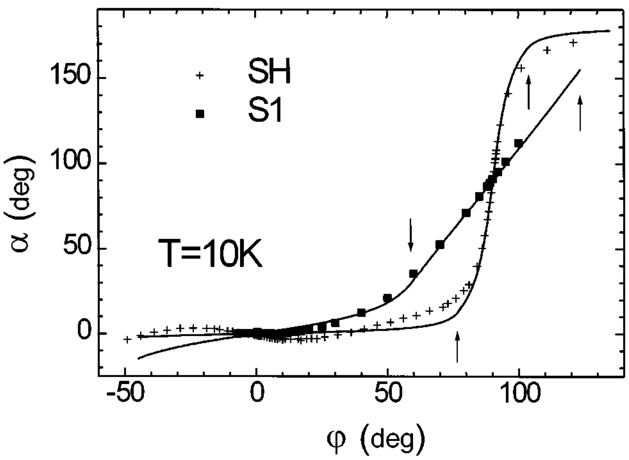

FIG. 4. Measured rotation of the magnetic moment (as in Fig. 2) of a $PbMoS_6$ sample ($T=10$ K, $\mu_0 H=1.0$ T) in its initial shape (No. SH), and after cutting to reduce the aspect ratio (No. S1). The full lines show the fits to Eqs. (3) and (6) calculated for aspect ratios κ of 4.3 and 1.69; the arrows mark the critical angles φ_c.

included here, its aspect ratio of $\sim 10^3$ yields a value for τ of $\sim 10^6$, well beyond our experimental resolution). Also, the coefficient of κ^2 is close to the value of 2/3 predicted by Eq. (12) for E-j characteristics of large n.

IV. GEOMETRICAL EFFECTS AND VORTEX BEHAVIOR IN HTS CRYSTALS

A. Angular scaling of magnetization curves

As we have seen, in magnetization measurements on HTS crystals, for a wide range of directions of **H** around the c axis, **m** remains parallel to the c axis, and so is dominated by the screening current density within the ab plane, $J_{(ab)}$. The magnitude of $J_{(ab)}$ (treating it for simplicity as a threshold, or Bean, critical current density) depends on the nature of the pinning force. In general, this dependence is nontrivial, but for weak isotropic disorder $J_{(ab)}$ should be constant for a fixed value of the scaled induction[15] $\varepsilon_\varphi B=(\cos^2\varphi +\Gamma^2\sin^2\varphi)^{1/2}B$, where Γ is the thermodynamic anisotropy; ε_φ is a fundamental parameter which determines the angular variation of the line energy of a vortex, of the upper critical field, of the melting transition, and of the irreversibility field B_{irr}.[15]

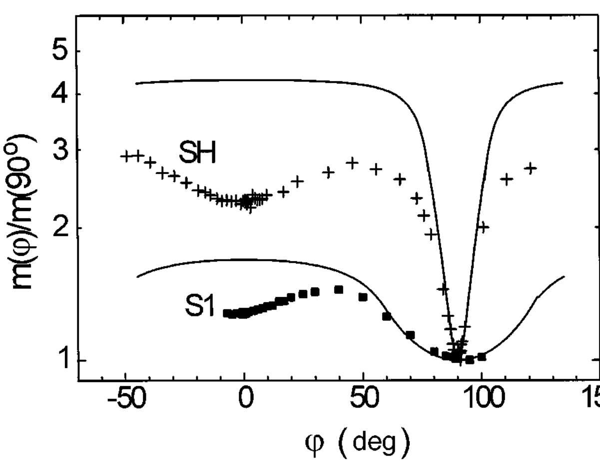

FIG. 5. Angular dependence of the magnetic moment modulus of the $PbMoS_6$ sample ($T=10$ K, $\mu_0 H=1.0$ T) in its initial state (No. SH), and after cutting (No. S1). The full lines show the fits $|\mathbf{m}|=\sqrt{(m_x^2+m_y^2)}$ to Eqs. (1), (2), (4), and (5) calculated for aspect ratios κ of 4.3 and 1.69.

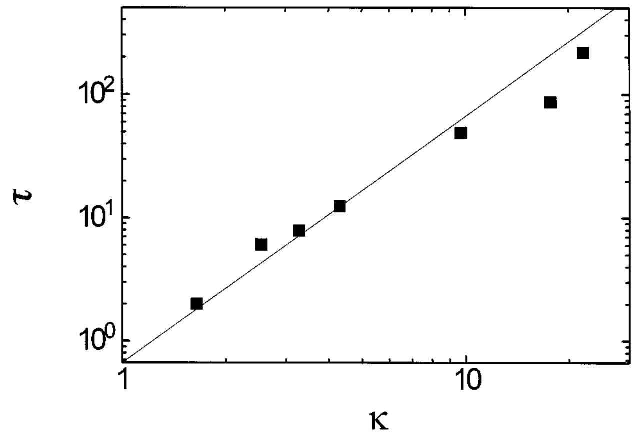

FIG. 6. Measured angular rotation rate τ of the magnetic moment when **H** passes through the plane of the plate, as defined by Eq. (7), for samples of a different aspect ratio κ. The full line is the prediction of the geometrical model, Eq. (7).

Consequently, if this scaling is valid, $|\mathbf{m}(\varphi)|$ measured at fixed values of $\varepsilon_\varphi H$ should be nearly constant as φ increases, decreasing to not less than 2/3 of its initial value at the angle φ_c (Sec. II A 2). The measurements on $YBa_2Cu_3O_7$ crystals (Fig. 7, where we have used a value for Γ^2 of 30, as found from linear plots of B_{irr}^{-2} against $\sin^2\varphi$) show that this is indeed the case for the detwinned sample No. MK. We include in Fig. 7 the prediction of the geometrical model for $|\mathbf{m}(\varphi)|$; it is clearly of the correct angular form, but there is a factor ~ 2 discrepancy between the calculated and measured ratios of the magnitudes of $|\mathbf{m}|$ at 0° and 90°.

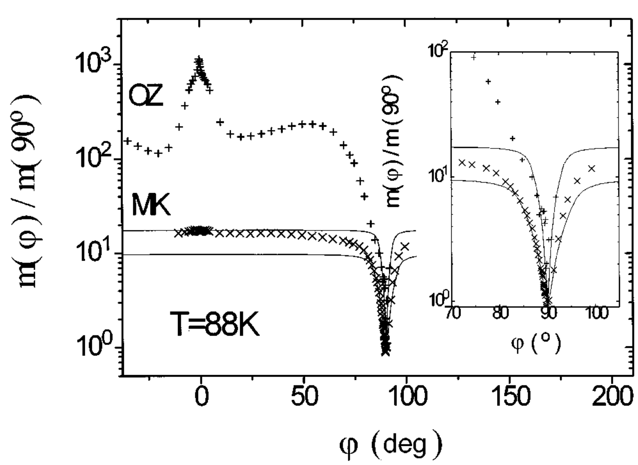

FIG. 7. Angular dependence of $|\mathbf{m}|$ for the detwinned No. MK and twinned No. OZ crystals at a fixed value of the scaled field $\epsilon_\varphi \mu_0 H=0.5$ T (calculated for $\Gamma^2=30$). The full lines show the fits of $|\mathbf{m}|$ to Eqs. (1), (2), (4), and (5) calculated for aspect ratios κ of 9.7 and 17.7. The strong peak around $\varphi=0$ in the No. OZ crystal is associated with vortex pinning to the twin planes, and occurs superimposed on the background geometric response. Inset: data in the vicinity of $\varphi=90°$.

On the other hand, in the twinned crystal No. OZ, $|\mathbf{m}(\varphi)|$ and so also $J_{(ab)}$, drop by an order of magnitude as $\mathbf{H}$ is rotated $\sim 20°$ away from the c axis. This behavior demonstrates the strong anisotropy of the vortex pinning associated with twin boundaries.

Another example of weak isotropic disorder is in the angular scaling of the ''fishtail'' peak in $YBa_2Cu_3O_7$ crystals seen by Klein *et al.*,[16] who measured $m(\varphi,B)$ at a succession of angles φ. They found empirically that the form of the peak obeyed the relation $m(\varphi,B/\cos\varphi)=\cos\varphi\, m(0,B)$ for angles up to $\sim 60°$ from the c axis. For the crystals studied in those experiments, with $\kappa \sim 8$, this angular range lies entirely within the regime of Sec. II A 2, in which $\mathbf{m}$ hardly deviates from the c axis. With a conventional (single-axis) magnetometer, as used by Klein *et al.*, the measured quantity is the component of $\mathbf{m}$ parallel to $\mathbf{H}$, in this situation equal to $|\mathbf{m}|\cos\varphi$; also, because Γ is at least 5 in $YBa_2Cu_3O_7$, over the measured angular range $\varepsilon_{\varphi}B \approx \cos\varphi\, B$. From these two angular dependencies, the observed scaling follows naturally. Consequently, this angular behavior of $J_{(ab)}$ supports association of the ''fishtail'' peak phenomenon with pinning by pointlike defects or their clusters,[10,17,18] which contribute weak isotropic disorder. However, other maxima of $J_{(ab)}$ with respect to B that do not scale in this manner are sometimes also seen; they presumably originate from other kinds of pinning centers, particularly twin boundaries.[17]

B. The analysis of critical current anisotropy

The HTS materials are strongly anisotropic, with the coupling between the superconducting CuO planes ranging from moderate in $YBa_2Cu_3O_7$ to extremely weak in the BiSrCaCuO phases. The thermodynamic anisotropy Γ increases from ~ 5 in $YBa_2Cu_3O_7$ to more than 20 in the BiSrCaCuO phases.

Here we are concerned with the question of measuring the anisotropy Ω of the (nonequilibrium) screening currents, defined as the ratio of the in-plane to out-of-plane critical current densities, $J_{(ab)}$ and $J_{(c)}$, respectively. This anisotropy is certainly influenced strongly by the thermodynamic anisotropy, but it includes also a significant contribution from the geometry of the pinning system that maintains the screening currents.

Because HTS crystals usually grow as quite thin platelets, with the crystallographic c axis normal to the plate, the geometric effects discussed earlier constrain the screening currents to flow within the ab plane, unless $\mathbf{H}$ is close, within an angle $\sim 1/\kappa$, to that plane. However, in order to obtain information about screening currents that flow parallel to the plate normal (or to the crystalline c axis), it is necessary but not *sufficient* to work within this window.

For fields applied along the symmetry directions of an anisotropic plate, the Bean model yields ''rooftop'' magnetic induction profiles.[19,20] Consider $\mathbf{H}$ applied in the ab plane of a HTS crystal, corresponding to the x direction in the analysis of Sec. II. There are two possibilities for flux penetration: In ''short'' samples with $L/t<\Omega$, flux penetrates faster along the z direction than along y, and m_x is dominated by the closure currents parallel to the c axis; only such samples are useful for the determination of Ω. In ''long'' samples with $L/t>\Omega$, flux penetrates faster in the y direction; in this case m_x is dominated by the in-plane z component $J_{(ab)}$ of the current density. Thus, in ''long'' samples, the y component $J_{(c)}$ of the current density is irrelevant.

Since HTS crystals are usually nearly square, with $w \sim L$, ''long'' and ''short'' are equivalent to κ greater and less than Ω, respectively. Measured values of Ω in fully oxygenated $YBa_2Cu_3O_7$ are in the range 5–10 (e.g., Refs. 12 and 13), smaller than κ for all the HTS samples measured here (Table I), so that these crystals are effectively ''long.'' Hence the important screening currents are always those that flow within the ab plane, and there is no need to introduce the complication of critical current anisotropy into our analysis. The agreement of the data with the geometric model when $\mathbf{H}$ is closely parallel to the ab direction, as shown by Fig. 6, confirms this conclusion.

Conversely, to obtain reliable information on the c-axis currents in $YBa_2Cu_3O_7$ by magnetic studies requires crystals of κ less than about 10, which are less common, and field alignment with the ab planes within a few degrees [Eqs. (4) and (5)]. In the more anisotropic HTS compounds, as-grown crystals may well have suitable aspect ratios, but the constraint on field alignment becomes rapidly more severe, and quickly surpasses the typical crystallographic mosaic spread of $\sim 0.1°$. It is for these reasons that magnetic measurements of the interplanar critical currents in HTS crystals yield quantitative results only over a rather narrow range of anisotropy.[12,13]

C. Vortex-locking phenomena in HTS

One of the most interesting phenomena predicted for HTS crystals is locking of vortices by planar (CuO planes or twin boundaries) or linear (irradiation columns) correlated pinning centers (see Ref. 15 and references therein). When the magnetic field is tilted away from the pinning system, the vortices remain locked to the plane or to the direction of the line defects. This behavior arises from the finite energy required for creation of the kinked vortex state, which is needed to accommodate vortex tilt. For locking by the CuO planes, the required energy is that for formation of a pancake vortex; for twin boundaries and columns, it is the formation energy of the connecting vortex segment. Only when the excess magnetic energy associated with tilting of the applied field reaches this energy threshold does the kinked structure form.

Consequently, the prime physical signature of vortex locking is the deviation of the vortices from the applied field direction, because of their adherence to the direction of the pinning system. In the vortex-locked state there is therefore complete shielding of the transverse component of $\mathbf{H}$, and so the generation of a *reversible* transverse magnetic moment. Previously used experimental approaches to the study of vortex-locking (e.g., Refs. 21–23) could not obtain information about the vortex direction, and so were unable to identify this phenomenon directly.

Recently, we have applied vector magnetometry to the vortex-locking problem.[24] The reversible transverse (to $\mathbf{H}$) magnetic moment of interest is inevitably accompanied by the irreversible moment induced by shielding currents. For the usual platelike crystal, the angular behavior of the irreversible moment is described by the geometric model discussed above. The twin boundaries run parallel to the c axis, and this is also the usual direction for columnar irradiation defects; vortex locking to these two defect species is therefore best studied by monitoring m_{ab} as $\mathbf{H}$ is rotated away from the c axis. In this geometry, we have seen that the irreversible moment remains closely locked to the c axis, and so gives negligible contribution to m_{ab}. Consequently, for twin boundaries or columnar defects parallel to the c axis, geometrical locking assists the observation of vortex-locking phenomena.

In contrast, for vortex-locking induced by the CuO planes, the associated reversible transverse moment is in the c direction, but it rapidly acquires a large irreversible contribution as $\mathbf{H}$ is rotated away from the ab plane [Eq. (5)]. Thus, geometrical effects tend to obscure the observation of vortex locking by the CuO planes. For example, they confuse rotation experiments[23] and cause the ideal transverse shielding to be dominated by the irreversible component. These effects have been demonstrated experimentally,[25,26] and will be discussed in more detail elsewhere.[27]

V. CONCLUSIONS

We have obtained the solution of the Bean model for an infinite thin plate in a tilted magnetic field, and discussed its extension to a more realistic description of a superconducting sample. For most of the angular range of the applied field $\mathbf{H}$, the magnetic moment $\mathbf{m}$ associated with the induced screening currents is almost locked to the plate normal, and the modulus of $\mathbf{m}$ changes very little. This locking has a purely geometrical origin, and is independent of any intrinsic superconducting anisotropy. However, when $\mathbf{H}$ approaches and then rotates through the plate plane, $\mathbf{m}$ changes direction and magnitude very rapidly.

The applicability of the geometric model has been investigated by vector measurement of the magnetic moment in a variety of HTS and conventional superconductor samples. We find very good agreement with the model in respect of the direction of $\mathbf{m}$, with locking to the plate normal over most of the angular range, followed by rapid rotation through the plate plane; the predicted variation of its magnitude is at least semiquantitatively correct.

We have shown that these geometric effects must be taken into consideration when exploring the anisotropy of critical current and vortex behavior in HTS crystals. In particular, there is an interplay between geometric locking of the irreversible magnetic moment and vortex-locking phenomena that assists the identification of vortex locking to twin boundaries, and also to other extended defects that run parallel to the c axis, but hampers severely the observation of vortex locking to the CuO planes.

ACKNOWLEDGMENTS

We are grateful to E. H. Brandt for several useful conversations, and to H. Küpfer for important discussions and providing us with the $PbMoS_6$ sample. We thank T. Wolf, M. Kläser, S. I. Krasnosvobodtzev, G. Wirth, and the late B. R. Coles for their provision of samples. This work was supported by NATO Linkage Grant No. HT931241, the UK Engineering and Physical Sciences Research Council, and the Russian Fund for Fundamental Research Grant No. 96-02-18376a.

APPENDIX A: THE MAGNETIC MOMENT ASSOCIATED WITH CLOSURE CURRENTS

The definition of the magnetic moment is

$$\mathbf{m}=\frac{1}{2}\int \mathbf{r}\wedge\mathbf{j}dV$$
$$=\frac{1}{2}\int [\mathbf{e}_x(j_z y-j_y z)+\mathbf{e}_y(j_x z-j_z x)+\mathbf{e}_z(j_y x-j_x y)]dV, \tag{A1}$$

where $\mathbf{e}_x$, etc., are Cartesian unit vectors.

It can be seen from Eq. (A1) that each component of $\mathbf{m}$ is determined by the sum of two contributions. We showed explicitly in Sec. II A how to calculate the contribution of the j_z current component to m_x and m_y in a long thin slab. We stated there that equal contributions arise from the closure currents j_x and j_y flowing at the ends, and we now prove this.

Consider a sample of arbitrary shape with time-independent shielding currents of density $\mathbf{j}$ flowing inside it; because of charge conservation $\mathrm{div}\mathbf{j}=0$, and therefore $\mathbf{j}$ is solenoidal. Consequently, the current distribution can be considered as made up from elemental current tubes carrying current i; each such tube is closed, and tubes do not intersect each other; note that we do not require the contour followed by the current tube to be planar.

The x component of the magnetic moment δm_x generated by an elemental current tube can be written, using Eq. (A1), as

$$\delta m_x=\frac{1}{2}\oint (s dl)(j_z y-j_y z), \tag{A2}$$

where s is the cross-sectional area of the current tube, and dl an element of its length; the line integral is taken around the contour followed by the current tube. In terms of a unit vector $\mathbf{e}_t$ in the direction of the element of current tube, $j_z=j\mathbf{e}_z\cdot\mathbf{e}_t$, the current i is sj, and $dz=dl\mathbf{e}_z\cdot\mathbf{e}_t$, so that

$$\delta m_x=\frac{1}{2}i\oint [dl(\mathbf{e}_x\cdot\mathbf{e}_t y-\mathbf{e}_y\cdot\mathbf{e}_t z)]=\frac{1}{2}i\oint (dz\,y-dy\,z). \tag{A3}$$

However, the projected area S_{yz} of the current tube is $\oint y\,dz\equiv-\oint z\,dy$, so that these two terms in Eq. (A3) contribute equally to δm_x, thus yielding the usual result with $\delta m_x=iS_{yz}$.

The first term in the integrand of Eq. (A2) is associated with current flowing in the z direction, which is the direction of the current flow in the central region of a long slab, as discussed in Sec. II A 2. The second term clearly represents the closure currents that flow at the ends of the slab. Since the two terms contribute equally in Eq. (A3), they do so also in Eq. (A2). As this equality holds for every elemental current tube, it must hold for the entire current distribution, and of course applies also to the other components of **m**, thus proving our statement about the contribution of the closure currents.

APPENDIX B: THE ELECTRIC FIELDS IN A SLAB INDUCED BY A TILTED TIME-DEPENDENT MAGNETIC FIELD

Within the framework of local electrodynamics, the electric fields and shielding currents in a superconductor can, in principle, always be calculated on the basis of Maxwell's equations and knowledge of the E-j characteristic;[28–30] however, the general case is intractable. For E-j characteristics independent of the magnetic field (as in the Bean model), and with the applied magnetic field increasing at a steady rate, the current distribution within the sample is stationary, so that the change of the magnetic induction is determined by the applied field **H** only. In an experimental context, this approximation is satisfied when there is negligible self-field, i.e., when **H** is large compared with the penetration field.

First we suppose that inside the superconductor there are no net electric charges, $\rho=0$ everywhere (later we will show that they can be created in certain cases). Then the electric fields are determined by the following equations:

$$\mathrm{div}\mathbf{E}=\mathbf{0} \tag{B1}$$

and

$$\mathrm{curl}\mathbf{E}=-\mu_0\frac{d\mathbf{H}}{dt} \tag{B2}$$

with the boundary condition for the normal electric field component $E_n=0$ at the sample surface.

Any continuous solution to these equations is necessarily unique.[31] It may be obtained as an infinite series of Green's functions, but the details are outside the scope of this paper. For an infinite slab with $\mathbf{H}\|y$ (Fig. 1), this solution simplifies greatly and we have

$$E_z=\mu_0\dot{H}_y x,$$
$$E_x=E_y=0. \tag{B3}$$

For a slab of finite length L, but still with $L>w$, we have to distinguish the end regions carrying the closure currents from the central region. The exact solution is too complicated to analyze, instead we use an approximation that is an exact solution for the Bean case. The boundaries that suggest themselves, and that accord with the superficial flux distribution seen in magneto-optic experiments,[28] are for $\mathbf{H}\|y$ the lines $z=L/2-w/2+x$ in the first quadrant and the three other symmetric diagonals (Fig. 8); similarly, for $\mathbf{H}\|x$, they are $z=L/2-t/2+y$, etc.

For $\mathbf{H}\|y$, Eq. (B2) is still satisfied in the central regions. At the ends, $L/2>|z|>L/2-w/2+|x|$, a solution is

$$E_x=-\mu_0\dot{H}_y\left(|z|-\frac{L}{2}+\frac{w}{2}\right)\mathrm{sgn}|z|,$$
$$E_z=E_y=0. \tag{B4}$$

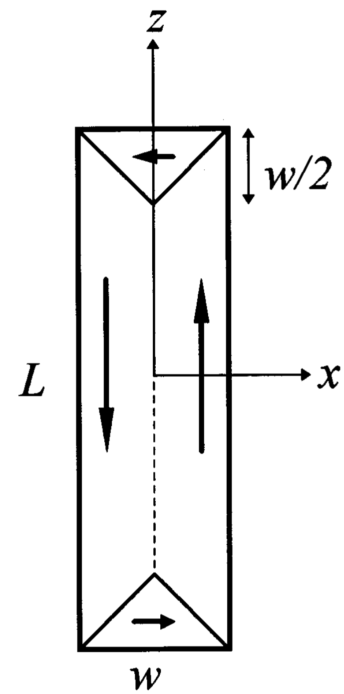

FIG. 8. Definition of the central and closure regions of a thin slab for **H** parallel to the y axis; bold arrows indicate the screening current direction.

The normal component E_n is continuous across the boundary between the two regions, so that there is no space charge. However, on the boundary itself curl**E** diverges because the components of the E field are unphysically discontinuous, thus violating Eq. (B2) We have examined numerical solutions of the problem, with **E** changing direction smoothly near the boundary line [and so still satisfying Eq. (B2)], but elsewhere similar to Eqs. (B3) and (B4). Since we are interested in a summation over the entire sample current distribution, we anticipate that these analytical discontinuities should not have significant impact on calculation of **m**.

For the other principal direction of the magnetic field, $\mathbf{H}\|x$, the solutions may be obtained by coordinate permutation; in the central region, we have

$$E_z=-\mu_0\dot{H}_x y,$$
$$E_x=E_y=0. \tag{B5}$$

In the closure regions, $L/2>|z|>L/2-t/2+|y|$, the solution is

$$E_y=\mu_0\dot{H}_x\left(|z|-\frac{L}{2}+\frac{t}{2}\right)\mathrm{sgn}|z|,$$
$$E_z=E_x=0. \tag{B6}$$

Because Eqs. (B1) and (B2) are linear, we may obtain **E** for any direction of **H** within the xy plane by summation of Eqs. (B3) and (B5) for the central region, and of Eqs. (B4) and (B6) for the closure regions.

For the central region of the finite slab ($|z|<L/2-w/2+|x|$ and $|z|<L/2-t/2+|y|$), and also for the infinite slab, we have an exact solution

$$E_z = -\mu_0 \dot{H}(y \sin\varphi - x \cos\varphi),$$
$$E_x = E_y = 0, \tag{B7}$$

where φ is the angle between **H** and the y axis.

In the closure regions of the finite slab the solutions are

$$E_x = -\mu_0 \dot{H}_y \left(|z| - \frac{L}{2} + \frac{w}{2} \right) \mathrm{sgn}|z| \quad \text{for } |z| \geqslant \frac{L-w}{2} + |x|, \tag{B8}$$

$$E_y = \mu_0 \dot{H}_x \left(|z| - \frac{L}{2} + \frac{t}{2} \right) \mathrm{sgn}|z| \quad \text{for } |z| \geqslant \frac{L-t}{2} + |y|, \tag{B9}$$

$$E_z = 0 \quad \text{for } |z| > (L/2 - w/2 + |x|) \text{ and } > (L/2 - t/2 + |y|),$$

$$E_z = \mu_0 \dot{H}_y x \quad \text{for } (L/2 - t/2 + |y|) < |z| < (L/2 - w/2 + |x|),$$

$$E_z = -\mu_0 \dot{H}_x y \quad \text{for } (L/2 - w/2 + |x|) < |z| < (L/2 - t/2 + |y|). \tag{B10}$$

The current distribution corresponding to these solutions for the **E** field can be obtained only in special cases. For the infinite slab, or the central region of a long slab, the Bean model E-j characteristic of $\mathbf{j} = j_c \mathbf{E}/E$ yields $j_z = \pm j_c$ as in Fig. 1, just as obtained in Sec. II A 2 from symmetry considerations. However, if the same description of the current density is applied to the closure regions of a finite slab in tilted magnetic field, charge conservation

$$\mathrm{div}\mathbf{j} = 0 \tag{B11}$$

is violated. Since we are dealing with steady-state solutions, this cannot be acceptable. We suggest that when the sweep of external field commences, there is a transient charge separation, so that in the steady state, Eq. (B11) is maintained, but Eq. (B1) now has $\mathrm{div}\mathbf{E} = \rho(\mathbf{r})$. These equations should then be solved with the boundary condition that the current density normal to the sample surface should be zero; that problem is beyond the scope of this paper.

The Ohmic case $\mathbf{j} = \sigma \mathbf{E}$, with an isotropic conductivity σ provides a much simpler situation; the solutions for **j** follow trivially from Eqs. (B3) to (B10) and Eq. (B1) guarantees $\mathrm{div}\mathbf{j} = 0$.

It is apparent that the ends of the slab always introduce intractable analytical complications; even in an Ohmic conductor, the boundary between the central and closure regions is difficult to describe. Although the E-j characteristic of a superconductor is very different from Ohmic, the analysis (Sec. II B) of power-law characteristics in infinite slabs shows that, as far as the magnetic moment is concerned, the difference between the Ohmic ($n = 1$) and Bean ($n \to \propto$) cases is only a numerical factor close to unity. Hence it is plausible that the angular behavior of the magnetic moment in a finite slab depends only very weakly on the real form of the E-j characteristic, and may be well approximated by the Ohmic result.

---

[*] Permanent address: General Physics Institute, Moscow 117942, Russia.

[1] W. Andrä, H. Danauand, and R. Hergt, Phys. Status Solidi **111**, 583 (1989).

[2] I. Felner, U. Yaron, Y. Yeshurun, G. V. Chandrashekhar, and F. Holtzberg, Phys. Rev. B **40**, 5239 (1989).

[3] L. Fruchter, C. Aguillon, S. Senoussi, and I. A. Campbell, Physica C **160**, 185 (1989).

[4] F. Hellman, E. M. Gyorgy, and R. C. Dynes, Phys. Rev. Lett. **68**, 867 (1992).

[5] Yu. V. Bugoslavsky, A. A. Minakov, and S. I. Vasyurin, J. Appl. Phys. **79**, 1996 (1996).

[6] C. P. Bean, Phys. Rev. Lett. **8**, 250 (1962).

[7] E. H. Brandt, Phys. Rev. B **49**, 9024 (1994).

[8] D. Lacey, R. Gebauer, and A. D. Caplin, Supercond. Sci. Technol. **8**, 568 (1995).

[9] Th. Wolf *et al.*, J. Cryst. Growth **96**, 1010 (1989).

[10] A. A. Zhukov, H. Küpfer, H. Claus, M. Kläser, and G. Muller-Vogt, Phys. Rev. B **52**, R9871 (1995).

[11] A. I. Golovashkin *et al.*, Physica C **162-164**, 715 (1989).

[12] V. V. Moshchalkov, A. A. Zhukov, V. A. Rybachyk, V. I. Voronkova, I. N. Goncharov, A. Yu. Martynkin, S. W. Moshkin, and I. N. Goncharov, Physica C **185-189**, 2191 (1991).

[13] J. V. Thomas, G. K. Perkins, D. E. Lacey, L. F. Cohen, A. D. Caplin, and V. I. Voronkova, Czech. J. Phys. **46**, 1775 (1996).

[14] H. Küpfer, A. A. Zhukov, A. Will, W. Jahn, R. Meier-Hirmer, T. Wolf, V. I. Voronkova, M. Kläser, and K. Saito, Phys. Rev. B **54**, 644 (1996).

[15] G. Blatter, M. V. Feigel'man, V. B. Geshkenbein, A. I. Larkin, and V. M. Vinokur, Rev. Mod. Phys. **66**, 1125 (1994).

[16] L. Klein, E. R. Yacoby, Y. Yeshurun, A. Erb, G. Müller-Vogt, V. Breit, and H. Wühl, Phys. Rev. B **49**, 4403 (1994).

[17] A. A. Zhukov, H. Küpfer, G. K. Perkins, L. F. Cohen, A. D. Caplin, S. A. Klestov, H. Claus, V. I. Voronkova, T. Wolf, and H. Wuhl, Phys. Rev. B **51**, 12 704 (1995).

[18] A. Erb, J.-Y. Genoud, F. Marti, M. Daumling, E. Walker, and R. Flukiger, J. Low Temp. Phys. **105**, 1023 (1996).

[19] E. M. Gyorgy, R. B. van Dover, K. A. Jackson, L. F. Schneemeyer, and J. V. Waszczak, Appl. Phys. Lett. **55**, 283 (1989).

[20] V. V. Moshchalkov, A. A. Zhukov, V. D. Kuznetsov, V. V. Metlushko, and L. I. Leonyuk, Superconductivity **2**, 84 (1989).

[21] P. A. Mansky, P. M. Chaikin, and R. C. Haddon, Phys. Rev. Lett. **687**, 2394 (1992).

[22] F. Steinmeyer, R. Kleiner, P. Müller, H. Müller, and K. Winzer, Europhys. Lett. **25**, 459 (1994).

[23] B. Janossy, A. Degraaf, P. H. Kes, V. N. Kopylov, and T. G. Togonidze, Physica C **246**, 277 (1995).

[24] A. A. Zhukov, G. K. Perkins, J. V. Thomas, A. D. Caplin, H. Küpfer, and T. Wolf, Phys. Rev. B (to be published).

[25] A. A. Zhukov, Yu. V. Bugoslavsky, G. K. Perkins, J. V. Thomas, A. D. Caplin, H. Küpfer, and T. Wolf (unpublished).

[26] Yu. V. Bugoslavsky, A. A. Zhukov, G. K. Perkins, A. D. Caplin, H. Kojima, and I. Tanaka, Phys. Rev. B (to be published).

[27] A. A. Zhukov, Yu. V. Bugoslavsky, G. K. Perkins, J. V. Thomas, A. D. Caplin, and H. Küpfer, T. Wolf (unpublished).

[28] E. H. Brandt, Phys. Rev. B **52**, 15 442 (1995); **54**, 4246 (1996).
[29] Th. Schuster, H. Kuhn, E. H. Brandt, M. V. Indenbom, M. Kläser, G. Muller-Vogt, H.-U. Habermeier, H. Kronmüller, and A. Forkl, Phys. Rev. B **52**, 10 375 (1995); Th. Shuster, H. Kuhn, and E. H. Brandt, *ibid.* **54**, 3514 (1996).
[30] A. A. Zhukov, Solid State Commun. **82**, 983 (1992); A. A. Zhukov, H. Küpfer, V. A. Rybachuk, L. A. Ponomarenko, V. A. Murashov, and A. Yu. Martynkin, Physica C **219**, 99 (1994); A. A. Zhukov, A. V. Volkozub, and P. A. J. de Groot, Phys. Rev. B **52**, 13 013 (1995).
[31] G. A. Korn and T. M. Korn, *Mathematical Handbook for Scientists and Engineers* (McGraw-Hill, New York, 1961).